Heliyon 9 (2023) e19415

Contents lists available at ScienceDirect

Heliyon

journal homepage: www.cell.com/heliyon

A multiband radio-frequency energy harvester for self-powered biosensor

Maissa Daoud [a,*], Hassene Mnif [a], Mohamed Ghorbel [b]

[a] Electronics and Information Technology Laboratory, University of Sfax, Tunisia
[b] Advanced Technologies for Medcine and Signals, University of Sfax, Tunisia

ARTICLE INFO

Keywords:
Multiband
Three-phase
RF-DC converter
Biomedical implant

ABSTRACT

This paper presents a novel nano-structure of radio frequency (RF) to direct current (DC) converter for the energy control unit in the biosensor. It is based on the Graëtz Bridge supplied with three-phase power (DP3). This circuit can be considered as the result of the proper combination of a common anode assembly and a common cathode assembly. In fact, the same three-phase converter structure was kept. The diodes have been replaced by six NMOS transistors connected in diodes. A number of capacitors have been added for each stage to boost voltage. The benefit of using this type of circuit is to obtain a powerful DC output signal with the smallest number of stages. The proposed architecture also enables MOS transistors to be driven by external 2.45 GHz voluntary signals originating from the implant's personal assistant. This would allow avoiding the use of transistor control circuits which are already power-consuming. For more power, the proposed converter receives two more involuntary global system for mobile signals (GSM) with 900 MHz and 1800 MHz frequencies bands in order to take advantage of the ambient energy. The proposed RF-DC converter efficiency reaches 62.8% for an input power equal to 10 dbm.

1. Introduction

In recent times, the progress of the biomedical field has facilitated or sometimes cancelled the intervention of the doctor. The speed of this evolution is explained by the complementarity of all the fields working on this project. These include the signal processing fields, standardized networks and protocols, energy conversion of all its forms, and the design and manufacture of circuits using nanotechnology [1]. An added benefit is the migration from the discrete to the integrated world through the invention of chemical materials and electronic and mechatronic components allowing the miniaturization of sensors for biomedical applications.

The use of biomedical implant is constantly increasing, which requires electronic circuit designers to meet the specifications imposed by the technological revolution and competition between micro-circuit manufacturers around the world [2,3]. This includes on the one hand the miniaturization of the blocks constituting the biomedical implant as well as the energy storage systems such as the battery, the capacitor and the supercapacitor [4]. It also involves the search for solutions in order to benefit from the ambient energy of all types whether solar, thermal, vibratory or even radio frequency (RF), to increase the battery span. Another solution is also possible and consists in avoiding any cable connection and resort to a wireless one. Improving the battery life of portable and miniaturized

* Corresponding author.
E-mail addresses: daoud_maissa@hotmail.com (M. Daoud), hassene.mnif@enetcom.usf.tn (H. Mnif), mohamed.ghorbel@enetcom.usf.tn (M. Ghorbel).

https://doi.org/10.1016/j.heliyon.2023.e19415
Received 5 April 2023; Received in revised form 16 July 2023; Accepted 22 August 2023
Available online 24 August 2023

devices is becoming a major challenge for increasingly sophisticated products [5,6].

The designers of biomedical implants have placed this objective at the top of the expected specifications. Several scientific studies will take place to decide on the appropriate energy source that can be recovered for a low-power micro-system. The availability of voluntary and involuntary RF signals on a continuous basis with low cost and small size manufacturing makes the RF energy the most common type used for low power devices. Several basic RF-DC converter structures are being used in previous and current research to improve the converter efficiency as well as; the RF-DC converter presented in Ref. [7], characterized by its high sensitivity, based on CMOS transistors and dedicated to the RFID band, the RF-DC converter described in Ref. [8], designed for biomedical applications, characterized by its low output power of around 307 μW, the RF-DC converter introduced in Ref. [9], developed on a CMOS transistor basis with threshold voltage compensation, and the DC RF-symmetrical energy collector demonstrated in Ref. [10], operated at the 2.45 GHz ISM band frequency to support the biosensor power supply unit.

In fact, the already mentioned vulnerabilities in the RF-DC energy converter raise new strategic, technological and conceptual challenges proposed in this work.

The remainder of this paper is structured accordingly: Section 2 presents the biomedical implant architecture and section 3 details the choice of the energy source. Sections 4, 5 and 6 explain respectively the choice of the standard, the proposed energy transfer strategy and the proposed input matching circuit. In Section 7, the proposed three phase RF-DC converter and the simulation results are summarized. The conclusions drawn from this study as well as our potential perspective are detailed in Section 8.

2. Biomedical implant architecture

A biomedical implant is a device whose task is to transform an observed physical measurement into an electrical measurement which in turn will be translated into binary data that can be used and interpreted by an informatics system [11]. It consists of a sensor equipped with a specific electronic circuit capable of measuring one or more physiological parameters. Biomedical implant architecture is represented in Fig. 1, which is composed of several elements or modules. Each module corresponds to a specific task of collecting and acquiring, processing or transmitting data. It also includes an energy source. Each implant consists of four units: the data acquisition unit (sensing unit and ADC (Analog Digital Converter)), the processing unit (processor), the communication unit (transceiver) and the energy control unit (power unit). The proposed research deals with the grey-coloured power supply block and specially the energy recovery.

A biomedical implant can be in one of four states: active in listening mode, active in data processing mode, active in transmission mode or not active in standby mode. It is in standby when its radio is turned off; in this case, its power consumption is almost zero. Indeed, the main source of energy consumption from an implant is the use of the wireless network via its radio communications. This consumption of energy has the potential to be reduced by decreasing data transmission.

3. Choice of energy source

Proper recovery of the energy contained in the system complies with these requirements: it ensures perfect autonomy if the proportion of energy recovered is high enough to guarantee the best possible consumption, even extending the battery's lifespan. There are countless candidate energy sources, each distinguished by the characteristics of the signal transmitted. Table 1 shows the energy density values of the sources commonly present in the environment.

According to Table 1, the RF radio frequency source is the right choice due to its high energy converted which may reach 100 μW/ cm3. In addition it is available all the time because of the enormous use of telecommunication systems. One more advantage is the integration in the implant since it is a micro system based on MOS transistors.

4. Choice of standard

The selection of a suitable wireless communication technology ultimately depends on the services offered, as well as the network designer's requirements. The parameters including energy consumption, flow rate, battery life, coverage range and number of nodes supported should all be considered. In Table 2, we compare the above-mentioned communication protocols. In our application, which is WBAN networks, we do not need a very large number of sensors in the network. On the other hand, low power consumption, long life

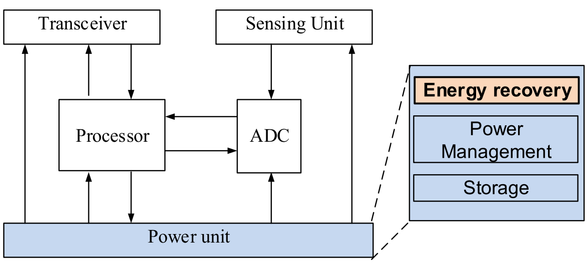

Fig. 1. Basic architecture of a biomedical implant.

Table 1
Comparison of the recoverable power density from different energy sources [12,13].

	Power density (μw/cm^3) over one year
Solar (Outdoor)	1000- Full sunshine
Solar (Indoor)	10
Vibrations/Movement (Human)	4
Acoustic noise	0.003@75dB, 0.96@100db
Temperature gradient	15- 10 °C gradient
RF (GSM) (μW/cm3)	0.1–100

battery, flow rate and range are very important factors in the case of remote medical monitoring.

Taking these constraints into account, ZigBee and Wibree technologies can be used to transmit medical data collected by sensors deployed on the human body to the collection node, i.e. in intra-BAN and inter-BAN communications. Indeed, these technologies offer low power consumption and a long range, but Wibree has an advantage over Zigbee due to its high data rate of 24 Mbit/s. For the proposed three-phase RF-DC converter, we used the Bluetooth for 2.45 GHz frequency as voluntary source and the GSM for 1800 MHz and 900 MHz frequencies bands, as involuntary source, because of its high-power transmission of about 30 dbm and availability everywhere.

5. Proposed energy transfer strategy

For additional RF energy harvesting, two scenarios are used as shown in Fig. 2. The first is based on ambient electromagnetic energy harvesting (EH: Energy Harvesting). The second scenario is based on Wireless Power Transfer (WPT), where a specific source ("Personal Digital Assistant") is employed for power delivery. Scenario one is suited to urban areas, for example, where power sources are increasingly available. In this instance, electromagnetic energy is available in all directions. A major benefit of the EH approach is the flexibility of antenna placement. However, as a result of legislated limits on exposure to electromagnetic fields and the indirect nature of transmitting antennas, the available power densities remain low for reception. Furthermore, power density is always influenced by the environment. Therein lies the greatest challenge for electromagnetic energy recovery. Add to this the limitations of the technological aspects of electronic components, making it extremely difficult to reach maximum efficiencies. To this effect, we have included the second scenario in our strategy to increase energy at the rectifier input and subsequently improve its efficiency.

6. Proposed input matching circuit

The proposed energy recovery is carried out at multiple frequencies concurrently, for greater efficiency. To this end, multi-band harvester has to be designed. In this case, two types of rectifiers can be used: the first uses a single adaptation circuit designed to operate on several frequency bands (Fig. 3) [20]. The second one uses several in parallel rectifiers, each of which is being designed for a different frequency.

Fig. 3(a) difficulty is to isolate one floor from the others when it comes to energy recovering at a particular frequency. On top of that, the use of two different communication scenarios requires the use of more than one antenna and this allows harvesting more energy. For this purpose, the matching circuit option presented in Fig. 3(b) was used for the impedance matching circuit at the input of the proposed converter.

In the electronic design of such an input impedance matching circuit, the power transferred between an electrical source and an electrical load depends on the voltage of the source and the impedances of both of the source (R_S) and the load (R_L) as displayed in Fig. 4.

The electrical efficiency of the system is the ratio between the power provided to the load (dissipated in R_L) and the total power delivered by the source (dissipated in R_L and R_S), it is expressed by equation (1).

$$\eta = \frac{P_L}{P_S} = \frac{1}{1 + \frac{R_S}{R_L}} \tag{1}$$

To maximize the transferred power (i.e., the power in the load), the impedances should be matched. To achieve such adaptation, the reactive part of the source impedance is first compensated (equation (2)). This requires that:

Table 2
Comparison between different wireless technologies [14–19].

Protocols	Bluetooth	UWB	Zigbee	GSM	WBAN
IEEE standard	802.15.1	802.15.3	802.15.4	GSM	802.15.6
Maximum theoretical flow rate (bits/s)	1–24 M	110–480 M	20-450 k	270.833 k	10 M
Frequency band (Hz)	2.4 G	3.1–10.6 G	2.4 G	900/1800 M	Several bands
Maximum theoretical range (m)	10	<10	10–100	35 k	5–10
Transmission power (dbm)	−20-20	20	18	30	Depends on bands

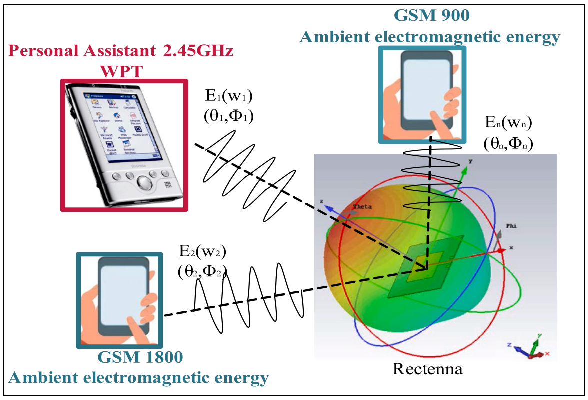

Fig. 2. Synoptic diagram of the proposed energy transfer strategy.

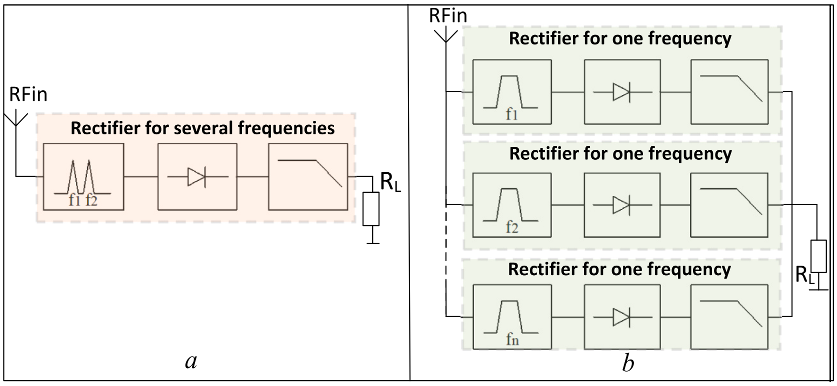

Fig. 3. The available multiband matching circuit options. a) Only one circuit for several frequencies. b) Several circuit for several frequencies.

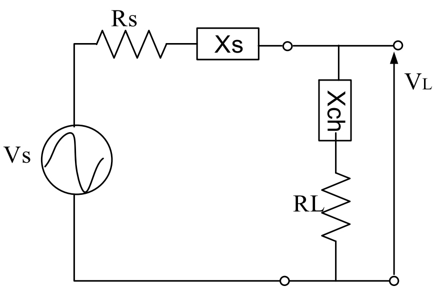

Fig. 4. Impedance matching electrical circuit.

$$X_{ch} = -X_S \tag{2}$$

subsequently, the resistive part of the load impedance should be equal to the resistive part of the source impedance. It is presented by equation (3).

$$R_{ch} = R_S \tag{3}$$

In a mathematical language, the two impedances are conjugated. In this case, the power dissipated in the load resistance is shown in equation (4).

$$p_{\max} = \frac{V_{eff}^4}{4R_S} \tag{4}$$

In the conception of the proposed circuit, it is considered: R_S as the antenna impedance and R_L as the impedance of the proposed RF-DC converter load. The adaptation is achieved through an LC network, which enables only the adaptation at the received signal frequency. There are several types of LC networks as: the L-circuit, the π-circuit and the T-circuit, summarized in Table 3. It is important to note that we have to wonder whether the load resistance be applied in parallel or in series. Both configurations serve for different purposes. In fact, if the first is used in the π-circuit, reserved for high load resistances, the second is applied in T-circuits and referred to in case of low resistances. Note that in both cases, the created resistance varies as the square of the impedance that controls it: if you double the impedance, you quadruple the resistance.

In reality, the filter is represented by an RLC circuit where the resistance R allows taking into accounts the losses in the inductance and the capacitor. The principle of the selective filter consists of exploiting the resonance of an RLC circuit (ideally LC). The transfer function of such a filter looks as shown in Fig. 5. The relative bandwidth of −3 db, Δω/ωo is given by equation (5).

$$\frac{\Delta w}{w_o} = \frac{1}{Q_C} \tag{5}$$

Qc represents the quality factor of the resonant circuit. It is limited by the losses in the capacitor and in the inductance, but more generally by those of the inductance if Qc = Lω/R. The production of highly selective filters therefore implies, in particular, the optimization of the inductance quality factor. Based on the RLC model presented in Fig. 6, the different parameters of the inductances used for this purpose were determined. This model takes into consideration the losses in the conductors, including those at high frequency, which results in a frequency-dependent RS resistance. It also considers capacitive couplings between turns and between turns and bonding (Cs) as well as capacitive couplings between the ground plane and the last turn.

The behaviour of the device is modelled by an ideal inductance Ls, an RS series resistor reflecting the Joule losses in the coil and the capacitance Cs in parallel on the assembly representing the capacitive couplings. The resistance Rs depends on the frequency and allows taking into account the skin effect, the proximity effects and the eddy currents in the turns. The elements of the model are determined from the elements of the admittance matrix below by equation (6).

$$Y_{11} = \frac{1}{R_s + jL_s w} + jC_s w \tag{6}$$

The elements of the equivalent model are presented by the following formulas (equation (7), (8) and (9)):

$$L_s = -\frac{\Im\left\{\frac{1}{Y_{11}}\right\}}{w} \tag{7}$$

$$R_s = \Re\left(\frac{1}{Y_{11}}\right) \tag{8}$$

$$f_0 = \frac{1}{2\pi\sqrt{L_0 C_s}} \tag{9}$$

The π-circuit was used for the proposed circuit adaptation. Fig. 7 shows the input reflection coefficient which has a good input adaptation of less than −10 dbm for the three frequencies: 2.45 GHz, 1.8 GHz and 900 MHz.

7. The three-phase RF-DC converter design

The proposed circuit is based on the Graëtz Bridge supplied with three-phase power (DP3). Its basic structure is shown in Fig. 8. This circuit can be considered as the result of the proper combination of a common anode assembly and a common cathode assembly. The benefit of using this type of circuit is to obtain a powerful signal with the least number of transistors. It also enables MOS transistors to be driven by external voluntary signals originating from the implant's personal assistant. This avoids the use of transistor control circuits which are already consumable of power.

Table 3
Different types of LC networks.

Types of LC networks	Schematic overview	Adaptation condition	Features
L-circuit	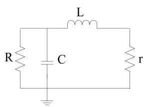	$r \cdot R = Z_L^2$	Adapts a low to high resistance
π-circuit	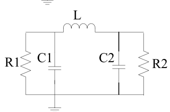	$\frac{R_1}{R_2} = \left(\frac{C_2}{C_1}\right)^2$	Suitable for high or medium resistances
T-circuit	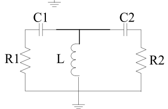	$\frac{R_1}{R_2} = \left(\frac{C_2}{C_1}\right)^2$	Adapts low to medium resistance

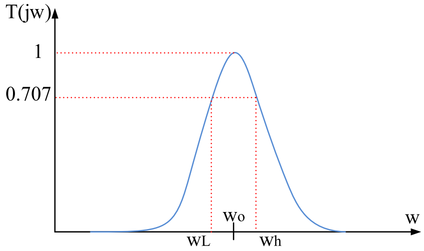

Fig. 5. Filter transfer function.

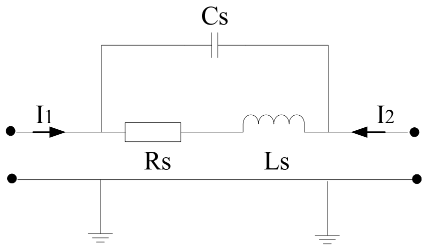

Fig. 6. RLC model inductance.

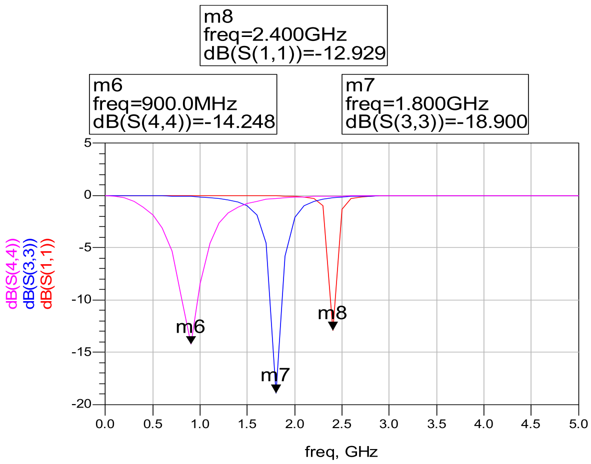

Fig. 7. Input reflection coefficient for 2.45 GHz, 1.8 GHz and 900 MHz frequencies.

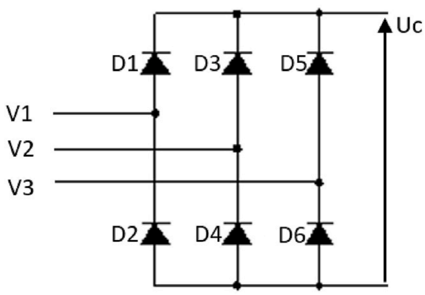

Fig. 8. Graëtz bridge three-phase basic structure.

The circuit operation is divided into six looped intervals. Two diodes (D1 and D4, D1 and D6, D3 and D6, D3 and D2, D5 and D2, D5 and D4) operate in each interval and generate an output voltage (Uc) at the load terminal as indicated in Fig. 9.

The proposed RF-DC converter is displayed in Fig. 10. It can be remarked that the same three-phase converter structure has been kept. The diodes have been replaced by NMOS transistors connected in diodes. A number of capacities have been added for each stage to perform the voltage boost function. The transistors are driven by the voltage Vin1 of source 1. The latter presents a voluntary signal of 2.45 GHz originating from the implant's personal assistant. This source is also controlled by the cognitive power control system designed for the rechargeable storage system. The output voltage for each stage is given by equation (10).

$$V_S(i) = \sum_{i=1}^{3} V_{in}(i) \tag{10}$$

For each stage the input voltage is summed to the rectified voltage of the previous stage. This is well described in Fig. 10.

The most important asset of the proposed converter is that it is externally controlled by the implant personal assistant through source one as shown in Fig. 10, i.e. the converter operates all the time as long as source one gives power whatever the power of the signals from sources two and three as shown in Figs. 11 and 12.

8. The three-phase RF-DC converter simulation results

The proposed three-phase RF-DC converter is implemented in TSMC 180 nm RF CMOS technology.

The variation of the output voltage for each stage over time is indicated in Fig. 13. The figure shows a better amplification moving from the first stage to the last stage. A zoom is applied to the curve of the output voltage variation versus input power in the time interval between 5 μs and 5.001 μs as is displayed in Fig. 14. The figure indicates that the increase in input power automatically causes the output voltage to increase.

The current collected at the converter output shows the sum of the incoming currents. As the current is directly proportional to the power, it undergoes the same increase as the voltage if the input power increases. This is shown in Fig. 15 and further detailed in Fig. 16.

In order to qualify the proposed RF-DC converter, the calculation of its percentage efficiency is necessary. The power efficiency of such a circuit is the quotient of the output power over the average input power. Two simulations are performed to test the proper performance of the circuit. The first is presented in Fig. 17, and shows the output power versus the output current for several input power values. The second is depicted in Fig. 18 reporting the circuit efficiency versus the output power. Efficiency may reach 62.8% for an input power equal to 10 dbm.

Table 4 summarizes the characteristics of the three-phase RF-DC converter described in this section. In comparison with other existing works, the three-phase RF-DC converter is stands out thanks to its powerful input and high efficiency close to 62.8% for a 10 dbm input.

9. Conclusion

A multiband RF-DC harvester with novel architecture has been developed in this paper. It is based on CMOS three-phase rectification to generate a powerful DC signal at the output. It allows benefiting from external 2.45 GHz voluntary signals and involuntary GSM signals with 900 MHz and 1800 MHz frequencies bands in order to improve energy harvesting. Its efficiency may reach 62.8% for an input power equal to 10dBm. The above considerations therefore open up considerable perspectives for our research work, and show that the use of the three-phase converter principle of discrete mode in the micro-integrated circuit feasible. The propose d system

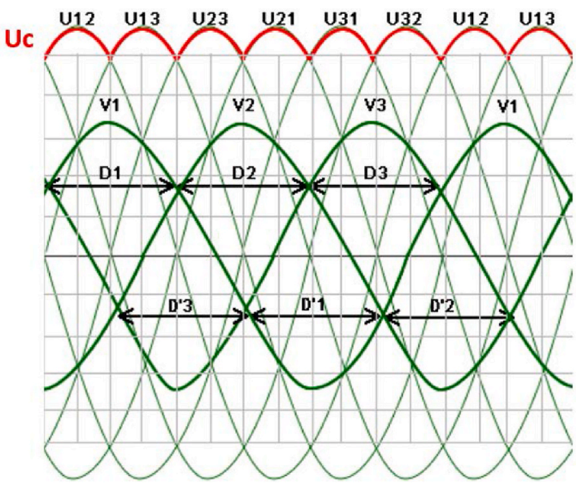

Fig. 9. Waveforms of the different voltages of a DP3 rectifier.

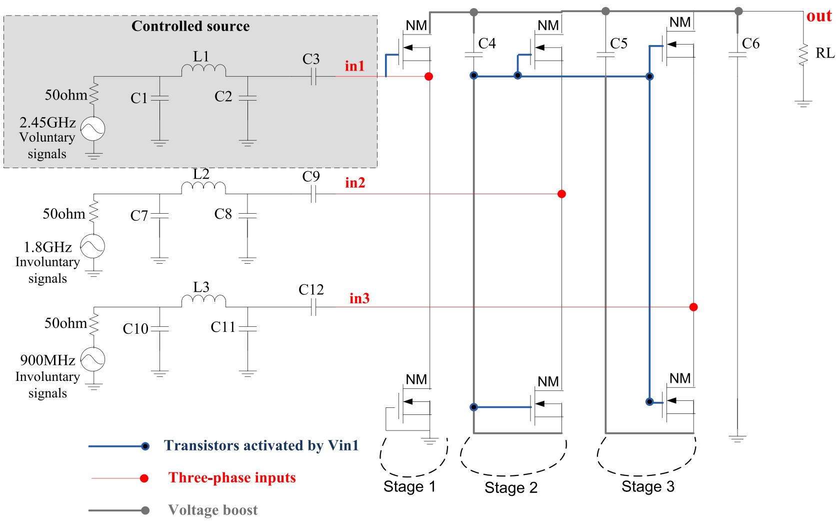

Fig. 10. The proposed RF-DC converter circuit: transistor level.

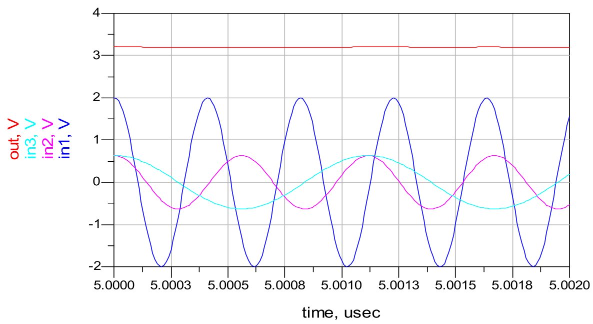

Fig. 11. Converter output voltage for inputs power; Pin1 = 2 dbm, Pin2 = 0 dbm and Pin3 = 0 dbm

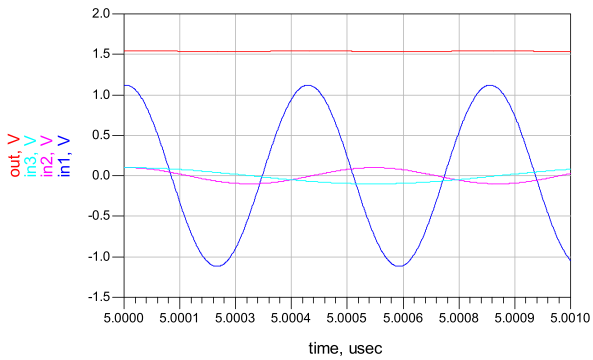

Fig. 12. Converter output voltage for inputs power; Pin1 = 0 dbm, Pin2 = −5 dbm and Pin3 = −5 dbm

could eventually be developed for intra-BAN applications (external biomedical sensors) and not just restricted to implants.

Author contribution statement

Maissa Daoud, Hassene Mnif & Mohamed Ghorbel: Conceived and designed the experiments; Performed the experiments; Analyzed and interpreted the data; Contributed reagents, materials, analysis tools or data; Wrote the paper.

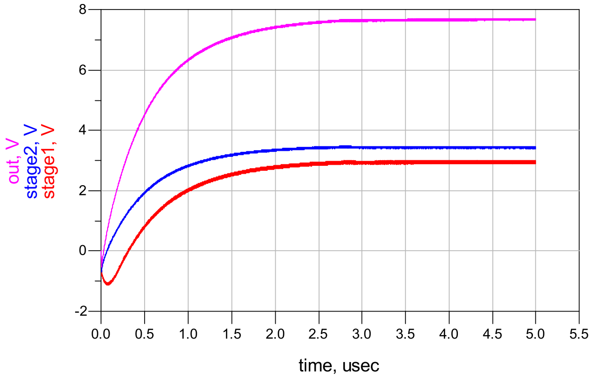

Fig. 13. Output voltage for each stage.

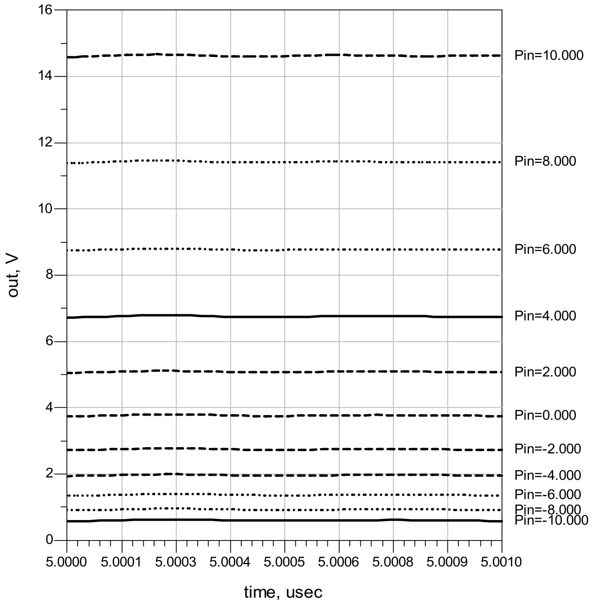

Fig. 14. Zoom on the variation of the output voltage versus the input power (dbm).

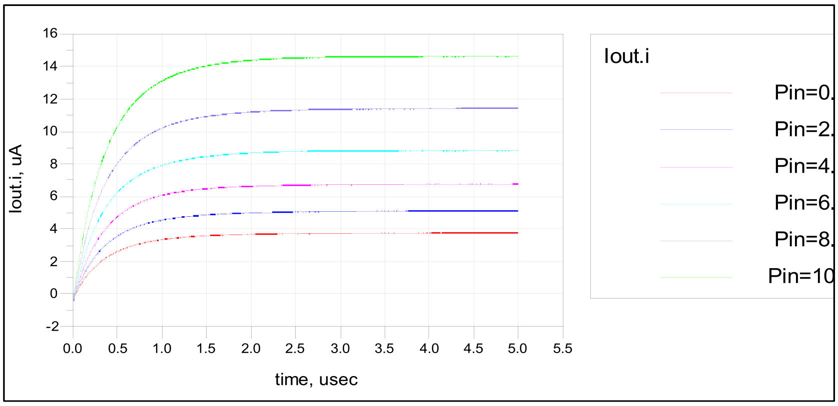

Fig. 15. Variation of the output current versus the input power (dbm).

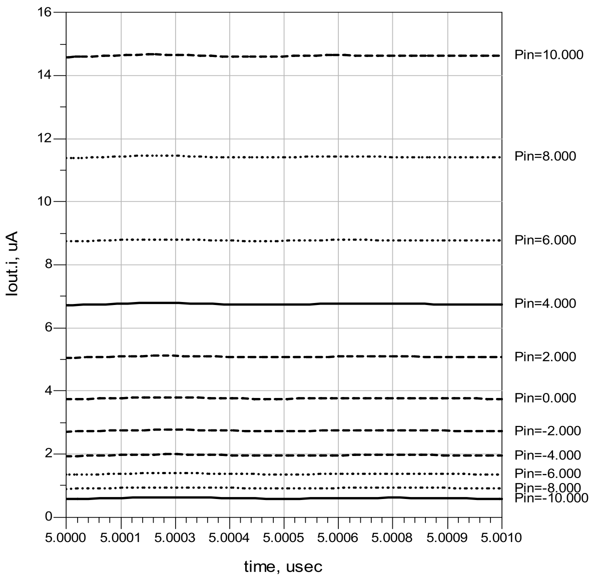

Fig. 16. Zoom on the variation of the output current versus the input power (dbm).

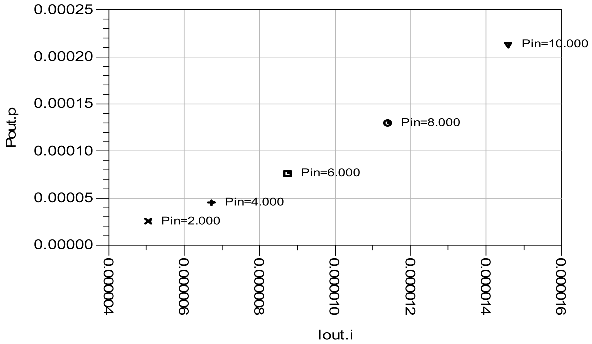

Fig. 17. Output power (dbm) versus output current (A) for several values of input power (dbm).

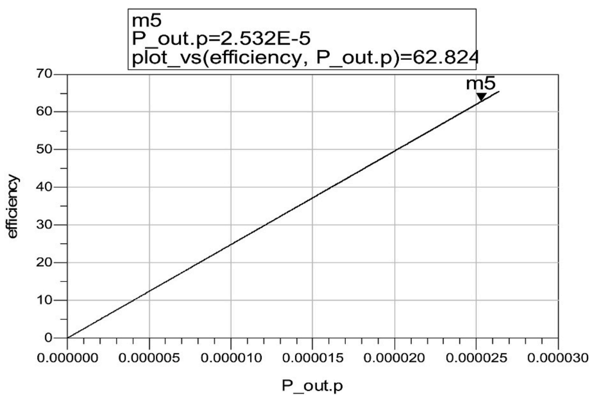

Fig. 18. Power efficiency (%) versus output power (dbm).

Table 4
Three-phase RF-DC converter Performance Comparison.

Design	This work	[10] 2021	[21] 2015	[22] 2015	[23] 2014	[24] 2017
Technology CMOS (nm)	180	180	300	180	180	180
Efficiency	62.8%	56%	23%	34%	47%	28.8%
Output Voltage(V)	1	1/-1	1.8	1	3.3	1.5
Min RF input (dbm)	10	0	0	−7	8.9	−9

Data availability statement

No data was used for the research described in the article.

Declaration of competing interest

The authors declare that they have no known competing financial interests or personal relationships that could have appeared to influence the work reported in this paper.

References

[1] H. Bai, X. Liu, Food nanotechnology and nano food safety, IEEE Nanotechnol. Mater. Devices Conf. Anchorage (2015) 1–4, https://doi.org/10.1109/NMDC.2015.7439261.
[2] A. Singh, A. Raj, A. Gupta, A. Tiwari, P. Kumar, Split ring resonator biosensor-an innovative design and analysis, IEEE Photon. Conf. Malaysia (2020) 117–118, https://doi.org/10.1109/ICP46580.2020.9206451.
[3] D. Tosi, A. Aitkulov, C. Molardi, M. Sypabekova, W. Blanc, Optical fiber biosensor based on an etched high-scattering fiber: towards reflector-less biosensors, IEEE International Workshop on Metrology for Industry 4.0 & IoT, Italy (2020) 260–263, https://doi.org/10.1109/MetroInd4.0IoT48571.2020.9138255.
[4] D.B.W. Abeywardana, B. Hredzak, V.G. Agelidis, Battery-supercapacitor Hybrid Energy Storage System with Reduced Low Frequency Input Current Ripple, International Conference on Renewable Energy Research and Applications Int. Conf, Renew. Energy Res. App., Palermo, 2015, pp. 328–332, https://doi.org/10.1109/ICRERA.2015.7418719.
[5] M. Daoud, M. Ghorbel, H. Mnif, A power control approach for a biosensor battery-supercapacitor storage system, J Storage Mater 43 (2021), e103166, https://doi.org/10.1016/j.est.2021.103166.
[6] H. Ko, S. Pack, Phase-aware directional energy transmission algorithm in multiple directional RF energy source environments, IEEE Trans. Veh. Technol. 68 (2019) 359–367, https://doi.org/10.1109/TVT.2018.2879723.
[7] R. Colella, M. Pasca, L. Catarinucci, L. Tarricone, S. D'Amico, High-sensitivity CMOS RF-DC converter in HF RFID band, IEEE Microw. Wireless Compon. Lett. 26 (2016) 732–734, https://doi.org/10.1109/LMWC.2016.2597212.
[8] Z. Liu, Y. Hsu, B. Fahs, M.M. Hella, An RF-DC converter IC with on-chip adaptive impedance matching and 307 μW peak output power for health monitoring applications, IEEE Trans Very Large Scale Integr VLSI Syst 26 (2018) 1565–1574, https://doi.org/10.1109/TVLSI.2018.2822120.
[9] O.Y. Al-Harbi, N.S. Al-Ghamdi, M.A. Al-Absi, S.R. Al-Batati, CMOS RF-DC Convertor for RF Wireless Energy Harvesting Based on Threshold Voltage Compensation, IEEE Regional Symposium on Micro and Nanoelectronics, Malaysia, 2019, pp. 12–15, https://doi.org/10.1109/RSM46715.2019.8943525.
[10] M. Daoud, H. Mnif, M. Ghorbel, A proposed 2.45 GHz RF-symmetrical DC energy harvester for the power unit in the biosensor, J. Circ. Syst. Comput. 30 (2021) 1–14, https://doi.org/10.1142/S0218126621501759.
[11] F.-G. Zeng, Challenges in improving cochlear implant performance and accessibility, IEEE Trans. Biomed. Eng. 64 (2017) 1662–1664, https://doi.org/10.1109/TBME.2017.2718939.
[12] S. Roundy, P.K. Wright, J. Rabaey, A study of low level vibrations as a power source for wireless sensor nodes, Comput. Commun. 26 (2003) 1131–1144, https://doi.org/10.1016/S0140-3664(02)00248-7.
[13] M. Raju, G. Mark, Ultra Low Power Meets Energy Harvesting, Texas Instrument, 2010, pp. 1–8.
[14] A.M. Robles-Cordero, W.J. Zayas, Y.K. Peker, Extracting the Security Features Implemented in a Bluetooth LE Connection, Int. Conf. Big Data, USA, 2018, pp. 2559–2563, https://doi.org/10.1109/BigData.2018.8622000.
[15] P. Cao, X. Hu, J. Wu, L. Zhang, X. Jiang, Y. Su, Reconfigurable UWB pulse generation based on a dual-drive mach–zehnder modulator, IEEE Photon. J. 6 (2014) 1–6, https://doi.org/10.1109/JPHOT.2014.2352632.
[16] G. Pan, J. He, Q. Wu, R. Fang, J. Cao, D. Liao, Automatic Stabilization of Zigbee Network, International Conference on Artificial Intelligence and Big Data, Chengdu, 2018, pp. 224–227, https://doi.org/10.1109/ICAIBD.2018.8396199.
[17] D. Suh, H. Ko, S. Pack, Efficiency analysis of WiFi offloading techniques, IEEE Trans. Veh. Technol. 65 (2016) 3813–3817, https://doi.org/10.1109/TVT.2015.2437325.
[18] M. Ibrani, E. Hamiti, L. Ahma, R. Halili, B. Dragusha, Comparative Analysis of Downlink Signal Levels Emitted by GSM 900, GSM 1800, UMTS, and LTE Base Stations, Annual Mediterranean Ad Hoc Networking Workshop, Budva, 2017, pp. 1–5, https://doi.org/10.1109/MedHocNet.2017.8001655.
[19] J. Park, Bio-inspired approach for inter-WBAN coexistence, IEEE Trans. Veh. Technol. 68 (2019) 7236–7240, https://doi.org/10.1109/TVT.2019.2917915.
[20] K. Niotaki, S. Kim, S. Jeong, A. Collado, A. Georgiadis, M.M. Tentzeris, A compact dual-band rectenna using slot-loaded dual band folded dipole antenna, IEEE Antenn. Wireless Propag. Lett. 12 (2013) 1634–1637, https://doi.org/10.1109/LAWP.2013.2294200.
[21] S.-T. Khang, J.-W. Yu, W.-S. Lee, Compact folded dipole rectenna with RF-based energy harvesting for IoT smart sensors, Electron. Lett. 51 (2015) 926–928, https://doi.org/10.1049/el.2015.0138.
[22] K. Gharehbaghi, O. Zorlu, F. Kocer, H. Kulah, Autocalibrating Threshold Compensation Technique for RF Energy Harvesters, IEEE RFIC symposium, Phoenix, AZ, 2015, pp. 179–182, https://doi.org/10.1109/RFIC.2015.7337734.
[23] C.J. Li, T.C. Lee, 2.4-GHz High-efficiency adaptive power, IEEE Trans Very Large Scale Integr VLSI Syst 22 (2014) 434–438, https://doi.org/10.1109/TVLSI.2013.2238264.
[24] Y. Chang, S.S. Chouhan, K. Halonen, A scheme to improve PCE of differential-drive CMOS rectifier for low RF input power, Analog Integr Circ S 90 (2017) 113–124, https://doi.org/10.1007/s10470-016-0825-y.